Measurement and Mitigation of the Ionosphere in L-band Interferometric SAR Data

Paul A. Rosen, Scott Hensley, Curtis Chen
Radar Science and Engineering Section
Jet Propulsion Laboratory, California Institute of Technology
Pasadena, CA 91109 USA
E-mail: Paul.A.Rosen@jpl.nasa.gov

***Abstract*— Satellite-based repeat-pass Interferometric Synthetic Aperture Radar (InSAR) provides a synoptic high spatial resolution perspective of Earth's changing surface, permitting one to view large areas quickly and efficiently. By measuring relative phase change from one observation to the next on a pixel-by-pixel basis, maps of deformation and change can be derived. Variability of the atmosphere and the ionosphere leads to phase/time delays that are present in the data that can mask many of the subtle deformation signatures of interest, so methods for mitigation of these effects are important. Many of these effects have been observed in existing ALOS PALSAR data [1], and studies are underway to characterize and mitigate the ionosphere using these data. Since the ionosphere is a dispersive medium, it is possible in principle distinguish the ionospheric signatures from the non-dispersive effects of deformation and the atmosphere. In this paper, we describe a method for mapping the ionosphere in InSAR data based on a multi-frequency split-spectrum processing technique.**

We examine a number of PALSAR data sets, including fully polarimetric and single-polarization 28 MHz bandwidth data, where anomalous effects in phase, amplitude and image registration have been observed. We demonstrate the estimation of the ionosphere by means of the split spectrum technique for estimating differential TEC, whereby a radar waveform is transmitted over the full PALSAR spectral band and widely separated portions of the receive spectrum are processed independently and compared for dispersive effects, and quantify its performance.

Introduction

The National Research Council (NRC) conducted a Decadal Survey of Earth Sciences [2] for NASA, and formulated a chronological plan for critical Earth Science missions to be flown over the next decade. The Survey recommended that NASA proceed with a number of missions immediately, one of which was called DESDynI (Deformation, Ecosystem Structure, and Dynamics of Ice), comprising both polarimetric a L-band radar operating as a repeat-pass interferometer and a multiple-beam lidar. These sensors will measure surface deformation for understanding natural hazards and climate and vegetation structure for understanding ecosystem health. The lidar needs to yield statistically-valid sampling of the Earth's vegetated surface over the life of the mission, and radar coverage needs to be at short (about 8 day) repeat intervals for resolution of rapid geophysical processes and for minimizing atmospheric delay variations in InSAR products. The radar should operate within the L-band portion of the spectrum, with large enough bandwidth to allow accurate ionospheric corrections. Horizontal spatial radar resolution should be about 10-20 m, the lidar spot size should be about 25 m, and vertical accuracies of the InSAR and lidar should be 1-2 mm and 2-10 cm, respectively. The major scientific objectives for DESDynI defined by the Decadal Survey are:

- Determine the likelihood of earthquakes, volcanic eruptions, and landslides
- Characterize the effects of changing climate and land use on species habitats and carbon budget.
- Predict the response of ice sheets to climate change and impact on sea level.
- Monitor the migration of fluids associated with hydrocarbon production and groundwater resources.

NASA has directed the Jet Propulsion Laboratory and Goddard Space Flight Center to conduct formulation trade studies to construct a feasible design that meets these science objectives within the programmatic constraints. These studies are well under way, and key performance and technical issues are being identified and addressed.

One of the key issues with L-band radar that is factoring into these trade studies is the quality of the data in the presence of ionospheric effects. Waves propagating through the atmosphere experience a variety of effects that depend on the total electron content (TEC) and at times the orientation of the magnetic field. These effects are generally described in terms phase delay, group delay, Faraday rotation, and amplitude and phase scintillations. Unlike the neutral atmosphere, which is non-dispersive (i.e. the refractive index

is not a function of frequency), the ionosphere is dispersive, and significant effects in the phase and time delay can be observed across the spectrum of a radar signal. In this paper, we describe a split-spectrum method to exploit the dispersive nature of the signal to estimate the contribution of the ionosphere, with the aim to remove the effects from the data.

I. Ionospheric Effects on Interferometric Phase

For the purpose of this paper, we are interested in addressing the effects of the ionosphere on the signal phase as it would appear in a SAR interferogram. In radar interferometry, two complex SAR images s_1 and s_2 are cross-correlated to form an interferogram $s_1 s_2^*$ (where * denotes complex conjugation), the phase of which represents the differential path delay between the two observations [3]. The differential two-way path delay is typically a combination of topographic parallax, any motion of the ground in between observations, and a refractive delay introduced by the atmosphere or the ionosphere:

$$\Delta\phi = \frac{4\pi}{\lambda}\frac{B_\perp}{r'}z + \frac{4\pi}{\lambda}\delta r_g + \frac{4\pi}{\lambda}\delta r_{atm} + \frac{4\pi}{\lambda}\delta r_{ion} \tag{1}$$

In Eq. 1, the first term is the simplified phase term proportional to the topography, where $B_\perp$ is the interferometric baseline, r' is a scaled version of the range, λ is the wavelength of the radar, and z is the topographic height. The second term represents the phase delay introduced if the ground moves by a distance projected into the radar line of sight (range direction) of δr_g. The third term represents the phase delay introduced if the neutral atmosphere produces a path delay difference between the two observations of δr_{atm}, and the fourth term represents the contribution due to the ionosphere for an equivalent ionospheric path delay difference between the two observations of δr_{ion}. As noted, the refractive index of the neutral atmosphere is non-dispersive, so δr_{atm} is a function of the integrated column of molecules along the radar paths at two different times and does not vary with wavelength at the wavelengths of interest. However, the ionospheric path delay difference δr_{ion} does, and can be described as

$$\Delta\phi_{ion} = \frac{4\pi}{\lambda}\delta r_{ion} = \frac{4\pi}{\lambda}\frac{K}{f^2}\Delta T_e = 4\pi\frac{K}{c^2}\lambda\Delta T_e \tag{2}$$

where here and in Eq. 1, the wavelength is taken to be the free-space wavelength. In Eq. 2, $K = 40.28$ m^3 s^{-2} and ΔT_e is the total electron content – the path integral of the electron density – along the radar line of sight. In Eqs. 1 and 2, the inherent difference in wavelength dependence between non-dispersive and dispersive components of the interferometric phase can be seen. Since the dispersive and non-dispersive components have different wavelength dependencies, it is possible to separate the effects by observing at multiple wavelengths. This is exploited routinely in GPS corrections of the ionospheric contributions, as well as a variety of other fields. For SAR applications, this property was used in testing the presence of dispersive effects in surface scattering from vegetation and rough lava [4].

This work was performed at the Jet Propulsion Laboratory, California Institute of Technology, under contract with NASA. Copyright 2009. All Rights Reserved.

For SAR, which inherently has a wide range bandwidth, the estimation technique amounts to sub-banding each observation in range and computing individual interferograms from each sub-band. By then scaling the difference properly an estimate of the ionospheric phase difference between observations can be determined, hence the ionospheric TEC difference, and also a non-dispersive phase difference estimate can be determined.

A. Estimation Method

Rewriting Eq. 1 in terms of non-dispersive and dispersive effects, using Eq. 2 as well,

$$\Delta\phi = \frac{4\pi}{\lambda}\delta r_{nd} + 4\pi\frac{K}{c^2}\lambda\Delta T_e \tag{3}$$

where δr_{nd} is the collection of non-dispersive terms in Eq. 1. If we divide the bandwidth of the data into two sub-bands centered at λ_1 and λ_2, then

$$\Delta\phi_1 = \frac{4\pi}{\lambda_1}\delta r_{nd} + 4\pi\frac{K}{c^2}\lambda_1\Delta T_e \tag{4}$$

$$\Delta\phi_2 = \frac{4\pi}{\lambda_2}\delta r_{nd} + 4\pi\frac{K}{c^2}\lambda_2\Delta T_e \tag{5}$$

Solving these two equations for δr_{nd} and ΔT_e,

$$\delta r_{nd} = \frac{\Delta\phi_2 - \frac{\lambda_2}{\lambda_1}\Delta\phi_1}{\frac{4\pi}{\lambda_1}\frac{\lambda_1}{\lambda_2} - \frac{\lambda_2}{\lambda_1}} \tag{6}$$

$$\Delta T_e = \frac{\Delta\phi_2 - \frac{\lambda_1}{\lambda_2}\Delta\phi_1}{\frac{4\pi}{\lambda_2}\frac{K}{c^2}\left(\lambda_2^2 - \lambda_1^2\right)} \tag{7}$$

Equations 6 and 7 provide the basis of the technique: by unwrapping the phase of sub-band 1, scaling by the wavelength ratio, then computing the difference between the phase of sub-band 2 and the scaled sub-band 1 phase, then unwrapping and scaling the result by the constant factor in the denominators, the non-dispersive and dispersive terms can be recovered. Note that difference in the numerator is typically very close to zero, so a formal unwrapping step is not necessary after forming the difference.

B. Estimation Issues

The estimation technique is expected to work well when the phase fringe variability is sufficiently low and the correlation of each interferogram is sufficiently high to allow unambiguous phase unwrapping to be possible. Phase unwrapping of at least one of the interferograms is needed

because the wavelength ratio must be applied to scale the phase of one before differencing in Eq. 6 or 7. Applying a non-integer scale factor to the wrapped phase will introduce non-integer phase discontinuities. Note that poor correlation due to temporal changes on the surface is not intrinsically an impediment to the technique, as the phase is generally difficult to interpret in these regions. These regions can generally be masked out in phase unwrapping algorithms. It is the combination of high fringe rates and decorrelation that leads to phase uwrapping errors generally.

Another issue with the technique is that the estimates are only relative differences, not absolute differences. Each interferometric phase can only be unwrapped to within a constant shift, that is the absolute phase of each interferogram is unknown. As a result, the difference phase can only be known to within a constant. Ground control or other knowledge of the state of the ionosphere (e.g. through models) can be used to estimate the constant.

The final issue is the noise inherent in these estimates. Note that the denominators of both Eqs. 6 and 7 involve differences of numbers that are nearly equal, so these differences are very small – for PALSAR, on the order of 1% of the values themselves. As a result, the phase differences computed are scaled up by a large factor, and noise as well as signal is amplified. Generally considerable amount of smoothing is needed to recover a usable signal.

II. Observations

A number of data sets have been examined, as shown in Table 1. L-band data (24 cm wavelength) is more sensitive to ionospheric effects than higher frequency systems, so the PALSAR data from JAXA's ALOS satellite provides numerous data sets to explore ionospheric effects. Indeed, many examples of these effects have been observed in PALSAR data [1].

TABLE I. PALSAR Observations

Site	Data Sets		
	Interferogram Dates	*Mode*	*Surface*
Antarctica	071125 / 080110	FBS	Ice motion
Sichuan	080408 / 080524	FBS	Co-seismic
Sichuan	090109 / 090224	FBS	Post-seismic
Alaska	070401 / 070517	Quad	Tundra/ Aurora

For the purposes here, we demonstrate with the Antarctic data set, located at (-73°, 107°). The FBS mode data of PALSAR have a range bandwidth of 28 MHz (32 MHz sampling frequency), at a center frequency of 1270 MHz. The split-spectrum processing used sub-bands at either end of the 28 MHz band with a bandwidth each of around 6 MHz.

Figure 1 shows the full resolution interferogram and interferometric correlation. Azimuth resolution is intrinsically less than 5 meters. Note the severe (blue) decorrelation bands. These are explained by rapid gradients in the phase along azimuth due to the ionosphere that lead to Doppler centroid differences. These in turn lead to relative pixel shifts that can cause decorrelation if not compensated. To ensure phase continuity, we processed the data to lower azimuth resolution. By doing so, the relative shifts relative to the resolution are smaller, and therefore the correlation remains higher.

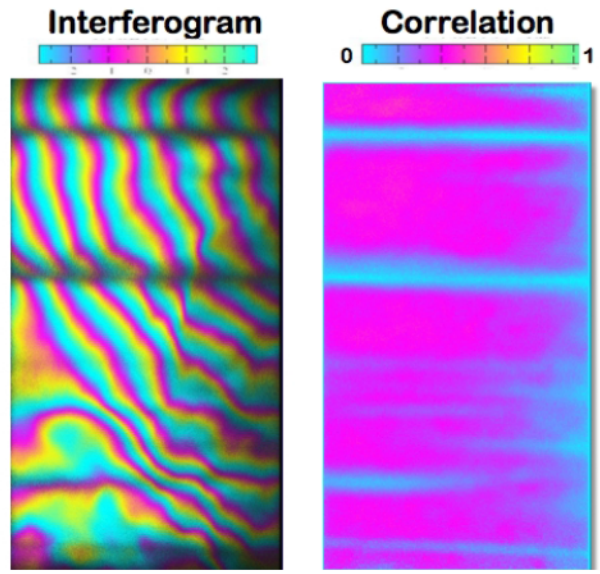

Figure 1. Full resolution interferogram (left) and correlation map (right). Note phase shear and decorrelation bands due to ionospheric gradients. Scale of images is approximately 80 km across and 140 km down.

Figure 2 illustrates the lower resolution processing in azimuth, to 20 m, applied to one of the 6 MHz side bands. At

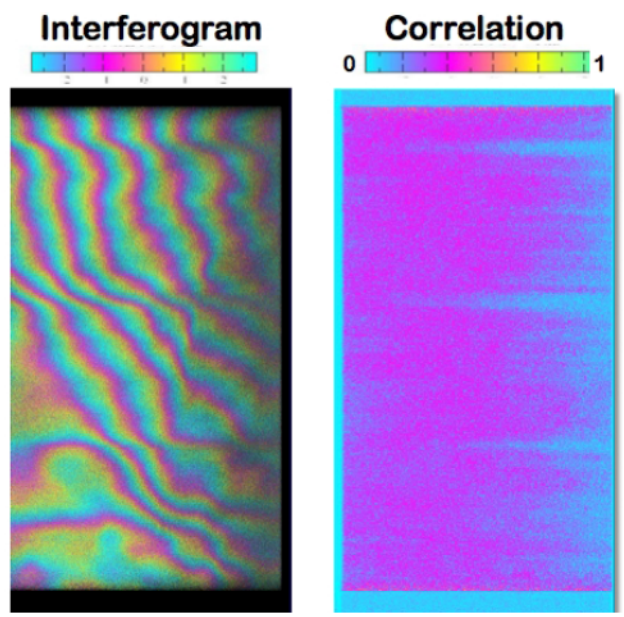

Figure 2. Side-band interferogram with 6 MHz bandwidth, processed to 20 m azimuth resolution, to improve correlation in regions of phase gradients. Note that the phase is continuous across regions that were previously decorrelated, at the expense of overall noise level. Scale of images is approximately 80 km across and 140 km down.

the scales shown, the relatively featureless fringes look approximately the same. The average noise level is higher, however the deep decorrelation bands have disappeared, and the phase discontinuities in Fig. 1 now appear as continuous sharp gradients in Fig 2.

III. Estimates of the Ionosphere

Figure 3 illustrates the application of Eqs. 6 and 7 to the two low resolution side-bands shown in Figure 1. The dispersive and non-dispersive terms are shown. Note that the phase scale on the color bar was stretched to draw out the effects, which are small in the differential interferograms. The non-dispersive phase is smooth and reminiscent of topography or motion, which makes sense geophysically. The dispersive phase on the other hand exhibits sharp gradients in range and azimuth that would explain the decorrelation bands.

More extensive processing of these data and the other data sets listed in Table I show similar effects. As an example, Figure 4 shows a more comprehensive processing of the Antarctic data shown in Figure 3, along with an estimate of relative Total Electron Content estimated from the data through Eq. 7. The plotted profile was obtained by averaging samples across-track in the center 25% of the image (roughly 400 pixels), reducing measurement noise further. This leads to along-track relative TEC estimates that have a standard deviation on the order of a few tenths of a TEC unit.

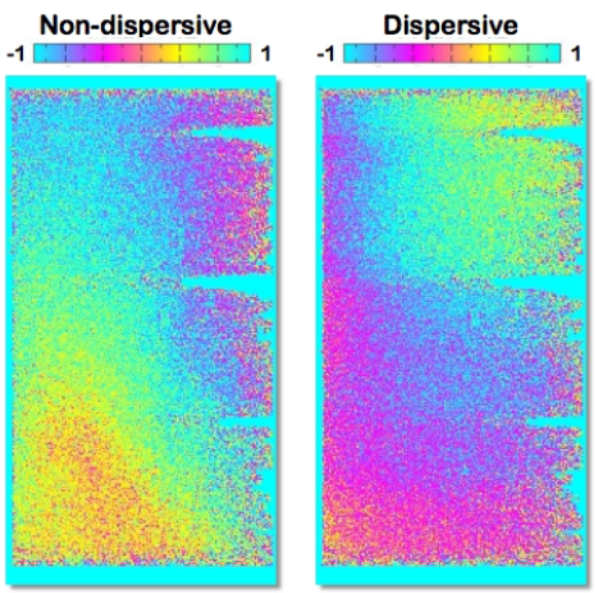

Figure 3. Estimates of the non-dispersive and dispersive phase associated with ionospheric effects. Note that the basic non-dispersive phase mimics the larger scale trend of the full res interferogram and is essentially continous and smooth across the areas where decorrelation exists due to phase shear. The dispersive phase estimate on the right however shows distinctly sharper gradients and variations that are atypical of surface processes. These are attributed to the differences in the ionosphere. Scale of images is approximately 80 km across and 140 km down.

IV. Mitigation

Once the estimate of the ionospheric phase is obtained, in principle two corrections can be made to the original data. The straightforward correction is to simply subtract the dispersive fringes from the original interferogram to remove the effect. The dispersive fringes must be averaged to reduce noise to an acceptable level, so some of the energy at the shortest spatial scales will remain. If the effect is large enough to introduce relative displacements between the two images leading to alignment mis-registration, then it would be advantageous to reconstruct a local warping function of one image relative to the other to re-form the interferogram at full resolution. The warping function in azimuth is related to the derivative of the ionospheric estimate in that dimension. In range, it is proportional to the phase directly. Note that the absolute relative geolocation of the pixels in the reference image (the image to which the relative warping function is not applied) may still be incorrect after this correction, because the absolute ionospheric signal of either image is not known.

V. Conclusion

In this paper, we have applied a common technique in remote sensing of comparing two frequency data to separate dispersive from non-dispersive effects in radar data. For SAR, we refer to this technique as the split-spectrum technique. We describe the basic equations as applies to SAR, and illustrate

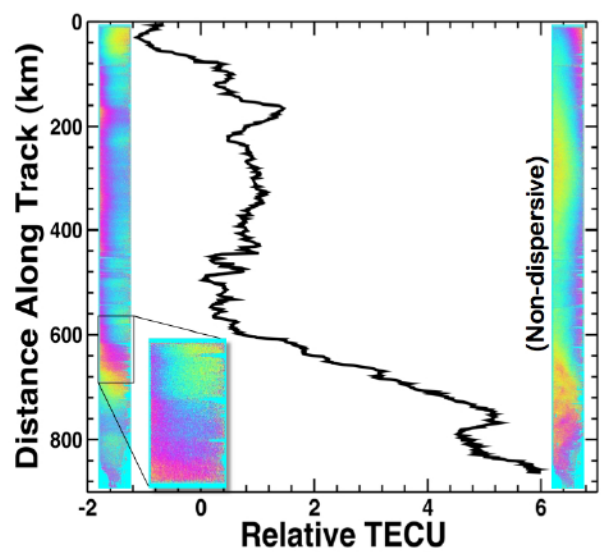

Figure 4. This is the same data set as Fig 3 (small inset lower left), but extending the processing to 900 km of the Antarctic ice sheet. On the left is the differential phase corresponding to the dispersive component of the differential propagation path. On the right is the non-dispersive component. At these scales, the difference between the irregular striations in the dispersive phase and the regular, presumably topographic, variations of the non-dispersive is apparent. Relative TEC, in TECU, is calculated from Eq. 7 and an along-track marginal profile is plotted above, showing significant spatial and temporal variability.

the technique with one example. The dispersive and non-dispersive effects show clear differences, with the non-dispersive phase – including what should be topography, topographic change, and atmosphere – showing smooth expected behavior, and the dispersive phase showing more variability. This technique shows promise for future L-band missions that exploit finer resolution and wider band separation, where the noise level in the estimates should be considerably lower. Once the map of dispersive effects is generated by this technique, it can be removed in principle from the original interferogram, ameliorating the error source.

Acknowledgment

This work was preformed at the Jet Propulsion Laboratory, California Institute of Technology, under contract with the National Aeronautics and Space Administration.

REFERENCES

[1] Meyer, F.J. Nicoll, J., The Impact of the Ionosphere on Interferometric SAR Processing, **Geoscience and Remote Sensing Symposium, 2008.**

[2] Earth Science and Applications from Space: National Imperatives for the Next Decade and Beyond, National Academy of Sciences, Washington, D.C., 2007.

[3] Rosen, P. A.; Hensley, S.; Joughin, I. R.; Li, F. K.; Madsen, S. N.; Rodriquez, E. & Goldstein, R. M., Synthetic Aperture Radar Interferometry, *Proc. IEEE,* **2000**, *88*, 333-382.

[4] Rosen, P. A.; Hensley, S.; Zebker, H. A.; Webb, F. H. & Fielding, E. J., Surface deformation and coherence measurements of Kilauea Volcano,Hawaii, from SIR-C radar interferometry, *J. Geophys. Res.,* **1996**, *268*, 1333-1336.